http://dx.doi.org/10.5012/bkcs.2013.34.6.1632

UV Enhanced NO_2 Sensing Properties of Pt Functionalized Ga_2O_3 Nanorods

Soyeon An, Sunghoon Park, Youngho Mun, and Chongmu Lee*

*Department of Materials Science and Engineering, Inha University, Incheon 402-751, Korea. *E-mail: cmlee@inha.ac.kr*
Received February 5, 2013, Accepted March 5, 2013

Ga_2O_3 one-dimensional (1D) nanostructures were synthesized by using a thermal evaporation technique. The morphology, crystal structure, and sensing properties of the Ga_2O_3 nanostructures functionalized with Pt to NO_2 gas at room temperature under UV irradiation were examined. The diameters of the 1D nanostructures ranged from a few tens to a few hundreds of nanometers and the lengths ranged up to a few hundreds of micrometers. Pt nanoparticles with diameters of a few tens of nanometers were distributed around a Ga_2O_3 nanorod. The responses of the nanorods gas sensors fabricated from multiple networked Ga_2O_3 nanorods were improved 3-4 fold at NO_2 concentrations ranging from 1 to 5 ppm by Pt functionalization. The Pt-functionalized Ga_2O_3 nanorod gas sensors showed a remarkably enhanced response at room temperature under ultraviolet (UV) light illumination. In addition, the mechanisms *via* which the gas sensing properties of Ga_2O_3 nanorods are enhanced by Pt functionalization and UV irradiation are discussed.

Key Words : Ga_2O_3, Nanorod, Gas sensor, UV, Functionalization

Introduction

Monoclinic gallium oxide (β-Ga_2O_3) is an important wide band gap semiconductor material. This material has potential applications in high temperature gas sensors[1-4] as well as transparent conducting electrodes,[5] phosphors,[6] and dielectric gates.[7] Recent studies on Ga_2O_3 gas sensors demonstrated that they detected O_2, H_2, CO, and CH_4 gases efficiently at high temperatures of 600-1,000 °C.[8,9] However, they demonstrated poor performance at room temperature. This high working temperature limits the practical use of Ga_2O_3-based gas sensors. Such high temperature operations are prone to induce ignition of flammable and explosive gases as well as high power consumption. Moreover, high temperature operation could lead to the long-term reliability problem due to the growth of the oxide grain. A range of techniques such as doping of novel metals,[10-12] MEMS fabrication,[13] nanosensing materials,[14] application of electrostatic field,[15] and ultraviolet (UV) irradiation[16-24] have been developed to reduce the operating temperature. Of these techniques, UV irradiation has attracted increasing attention as a promising strategy. Since Camagni et al.'s report on UV-enhanced semiconducting oxide sensors,[12] many researchers have reported that UV irradiation improved the sensing performances of semiconducting oxide gas sensors.[16-23] On the other hand, there is almost no report on the gas sensing properties of one-dimensional nanostructures functionalized with metal catalyst under UV illumination. This study examined the NO_2 gas sensing properties of networked Pt-functionalized Ga_2O_3 nanorods at room temperature under UV illumination to see the possibility of the practical use of Ga_2O_3-based gas sensors at room temperature.

Experimental

Pt-functionalized Ga_2O_3 nanorods were synthesized by the synthesis of Ga_2O_3 nanorods by the thermal evaporation of GaN powders followed by the sputter-deposition of Pt and thermal annealing. Au-coated Si was first used as a substrate for the synthesis of 1D Ga_2O_3 structures. Au was deposited on the (100) Si substrate by direct current (dc) sputtering. A quartz tube was mounted horizontally inside a tube furnace. The 99.99% pure GaN powders were placed on the lower holder at the center of the quartz tube. The Au-coated Si substrate was placed on the upper holder about 5 mm apart from the GaN powders. The furnace was heated up to 1,000 °C and maintained at the temperature for 1 h in N_2/3 vol %-O_2 atmosphere with constant flow rates of oxygen (O_2) (10 sccm) and N_2 (300 sccm). The total pressure was set to 1.0 Torr. Next, a thin Pt film was deposited onto the surfaces of some of the as-synthesized β-Ga_2O_3 nanorod samples using a direct current (dc) sputtering technique (substrate temperature: room temperature, power: 20 mA, working pressure: 1.9×10^{-2} Torr, and process time: 180 sec). The Pt-coated nanorods were then annealed at 800 °C for 30 min in an Ar atmosphere. The Ar gas flow rate and process pressure were 100 standard cubic centimeters per minute (sccm) and 0.8 Torr, respectively. The morphology and structure of the collected nanorod samples were characterized using a scanning electron microscope (SEM, Hitachi S-4200) operating at 10 kV and a transmission electron microscope (TEM, Philips CM-200) with an accelerating voltage of 300 kV. The energy-dispersive X-ray (EDX) elemental analysis was carried out using a JED-2300 EDX system fitted to the TEM. The crystallographic structure was determined by glancing angle X-ray diffraction (XRD, Philips X'pert MRD diffractometer) using Cu K_α radiation ($\lambda = 0.15406$ nm) at a scan rate of 2°/min. The sample was arranged geometrically at a 0.5° glancing angle with a rotating detector.

Multiple networked Pt-functionalized Ga_2O_3 gas sensors were fabricated by pouring a few drops of nanorod-suspended NO_2 onto SiO_2 (500 nm)/Si substrates equipped with a

pair of IDEs with a gap of 20 μm. The sensor was tested for its response to NO_2 using a home-built computer-controlled characterization system. The chamber was designed to hold the sample to a four-point probe configuration firmly while maintaining the gas composition under investigation. The chamber was connected to the gas inlet line coming from the mass flow controllers. Two mass flow controllers (MFCs) were used in combination with a controller to control the NO_2 flow rate. A gas exhaust tube was located at the opposite side of the chamber. The flow-through technique was used to test the gas-sensing properties of the pristine and Pt-functionalized Ga_2O_3 nanorods. All the measurements were executed in a temperature-stabilized sealed chamber at room temperature under controlled humidity. The test gas was mixed with synthetic air of 0.5 L/min to achieve the desired concentration, and the flow rate was maintained at 200 standard cubic centimeter per minute (sccm) using mass flow controllers. National Instruments Labview™ program was used to control the mass flow controllers, meter and record the NO_2 concentration. A Keithley sourcemeter-2612 was used to acquire the impedance data. The sourcemeter was hooked to a computer *via* a GPIB cable and this data was also acquired using the LabView™ software. The electrical resistance of gas sensors was determined in the dark and under UV light ($\lambda = 365$ nm) illumination at 1.2 mW/cm^2 by measuring the electric current at room temperature that flowed when a potential difference of 5 V was applied between the Ni (~10 nm)/Au (~50 nm) interdigited electrodes. The response R is defined as R (%)) $R_g/R_a \times 100$, where R_a is the resistance of the sensors in air ambience, and R_g is the resistance of the sensors in NO_2 gas.

Results and Discussion

Figure 1 shows a SEM image of the Pt-functionalized Ga_2O_3 nanorods prepared by thermal evaporation followed by sputtering. It shows that the synthesis scheme adopted in this study can grow Ga_2O_3 nanorods with diameters of 50-250 nm and lengths up to a few hundreds of micrometers.

The EDX spectrum (Figure 2(a)) and EDXS elemental image map (Figure 2(b)) of a typical Pt-functionalized Ga_2O_3 nanorod confirmed that the Pt-functionalized Ga_2O_3 nanorod was composed of Ga, Pt and O (Figure 2(a)). The Cu in the spectrum was assigned to the TEM grid. The low-magnification TEM image shows a typical Pt-coated Ga_2O_3 nanorod with a thickness of approximately 120 nm (Figure 3(a)). Fringe patterns were observed all over the whole HRTEM image of the Ga_2O_3 nanorod (Figure 3(b)). The resolved spacing between two neighboring parallel fringes were approximately 0.37 and 0.21 nm, which were in good agreement with the interplanar spacings of the {201} and {311} planes of bulk β-Ga_2O_3 crystals (JCPDS No. 87-1901, a = 1.221 nm, b = 0.304 nm, c = 0.580 nm, and β = 103.8°), respectively. The corresponding selected area electron diffraction (SAED) pattern recorded perpendicular to the long axis, were indexed for the [$\bar{1}$12] zone axis of β-Ga_2O_3.

The reflection spots in the corresponding selected area

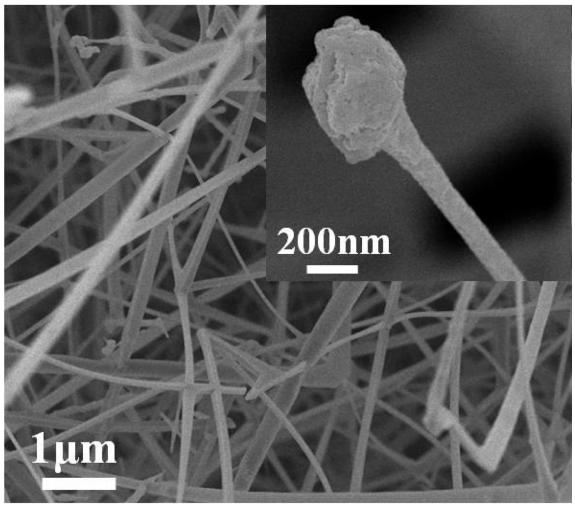

Figure 1. SEM image of Pt-functionalized Ga_2O_3 nanorods. Inset, enlarged SEM image of a typical Pt-functionalized Ga_2O_3 nanorod.

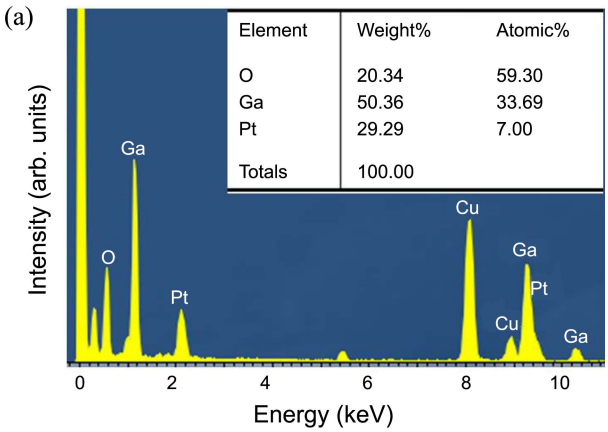

Figure 2. (a) EDX spectrum of the central region of a typical Pt-functionalized Ga_2O_3 nanorod. (b) EDXS elemental image maps.

electron diffraction (SAED) pattern (Figure 4(c)) were identified to be (110), (201) and (311) reflections of monoclinic-structured Ga_2O_3, indicating that the Ga_2O_3 nanorod in the TEM image is a single crystal. The XRD pattern of the as-

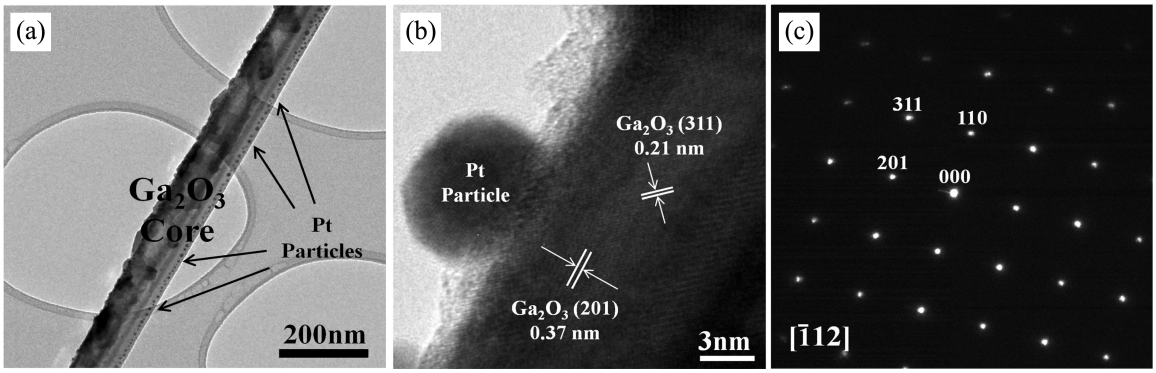

Figure 3. (a) Low magnification TEM image, (b) high-resolution TEM image, and (c) selected area electron diffraction pattern of Pt-functionalized Ga_2O_3 nanorods.

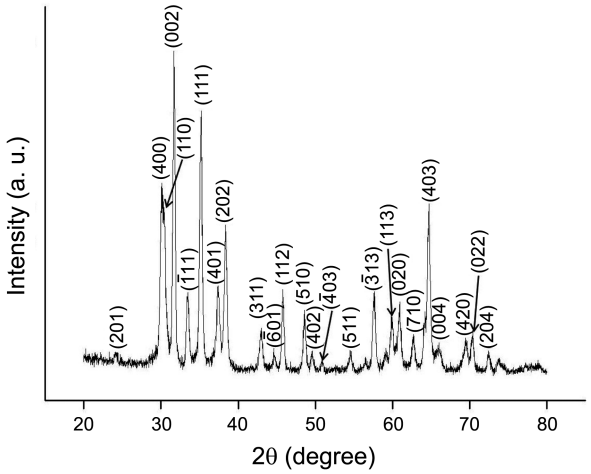

Figure 4. XRD patterns of Pt-functionalized Ga_2O_3 nanorods.

Table 1. Responses measured at different NO_2 concentrations for the Pt-functionalized Ga_2O_3 nanorod sensor at room temperature under UV illumination at 1.2 mW/cm^2

NO_2 Conc.	Response (%)	
	Ga_2O_3	Pt-Ga_2O_3
1 ppm	143.08	255.27
2 ppm	162.51	318.27
3 ppm	195.81	480.25
4 ppm	247.21	675.28
5 ppm	297.85	930.97

synthesized Pt-functionalized Ga_2O_3 nanorods is presented in Figure 4. The main diffraction peaks in the pattern of the as-synthesized nanorods can be indexed to the lattice planes of a monoclinic structured-single crystal β-Ga_2O_3, indicating that the nanomaterial is β-Ga_2O_3.

Figure 5(a) shows the sensing characteristics of the Pt-functionalized Ga_2O_3 nanorods at room temperature toward NO_2 gas under the illumination of UV light at 1.2 mW/cm^2. Both the pristine and Pt-functionalized Ga_2O_3 nanorod sensors exhibited good response/recovery cycle to the NO_2 gas pulses and the sensor responses increased with increasing gas concentrations. Multiple networked pristine Ga_2O_3 nanorods showed responses ranging from 143, to 298% at NO_2 concentrations of 1-5 ppm (Table 1). In contrast, the Pt-functionalized Ga_2O_3 nanorods showed responses ranging from 255 to 931% in the same concentration range (Table 1). Therefore, the response of the nanorods was improved 2-3 fold at each NO_2 concentration by the functionalization of Ga_2O_3 nanorods with Pt. Figure 5(b) and (c) show the enlarged parts of the data in Figure 5(a) measured at an NO_2 concentration of 5 ppm for the pristine Ga_2O_3 and Pt-functionalized Ga_2O_3 nanorods, respectively, to reveal the moments of the gas input and gas stop. The resistance increased upon exposure to NO_2 and recovered completely to the initial value upon the removal of NO_2. The sensor responses to NO_2 gas were also stable and reproducible for repeated test cycles.

Figure 6 shows the dynamic responses of the Pt-functionalized Ga_2O_3 nanorods to 5 ppm NO_2 gas at room temperature under the illumination of the UV lights with different illumination intensities. The dynamic response of the Pt-functionalized Ga_2O_3 nanorods at room temperature without UV light illumination *i.e.*, for the UV intensity of 0 mW/cm^2 is not shown in Figure 6 purposely because the change in resistance was negligible and unstable.

Table 2 shows that the response of the Pt-functionalized Ga_2O_3 nanorods increased from 175 to 931% with increasing the UV light illumination intensity from 0.35 to 1.2 mW/cm^2. These high responses at room temperature prove the strong influence of UV light irradiation on the response of the nanosensor toward NO_2 gas. In other words, this result supports previous reports that the UV light irradiation technique can realize room temperature-gas sensors.[12-20]

The NO_2 gas sensing mechanism of the Pt-functionalized Ga_2O_3 nanorods under UV light illumination can be depicted as follows: When the nanorods are exposed to air, it interacts with oxygen by transferring electrons from the conduction band to the adsorbed oxygen atoms, forming ionic species, such as O^-, O^{2-} and O_2^-, as shown in the following reactions:[25,26]

$$O_2\,(g) \rightarrow O_2\,(ads) \quad (1)$$

$$O_2\,(ads) + e^- \rightarrow O_2^-\,(ads) \quad (2)$$

$$O_2^-\,(ads) + e^- \rightarrow 2O^-\,(ads) \quad (3)$$

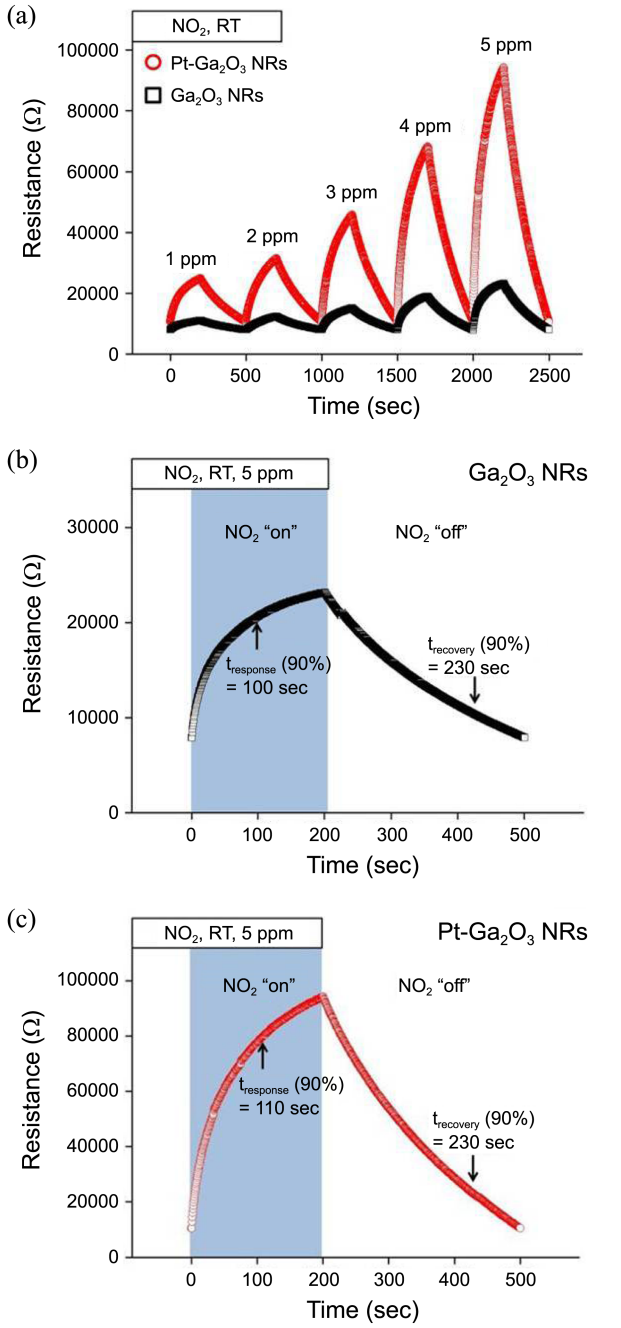

Figure 5. (a) Dynamic responses of pristine and Pt-functionalized Ga_2O_3 nanorods to NO_2 gas ranging from 1 to 5 ppm at room temperature under UV light illumination (b) Enlarged part of the pristine Ga_2O_3 nanorod curve in Figure 5(a) at 5 ppm NO_2. (c) Enlarged part of the Pt-functionalized Ga_2O_3 nanorod curve in Figure 5(a) at 5 ppm NO_2.

$$O^- (ads) + e^- \rightarrow O^{2-} (ads) \quad (4)$$

A depletion layer is created in the surface region of the nanorods because electrons in the surface region of the nanorods are consumed, resulting in a decrease in the electrical resistance in the nanorods. Upon exposure to UV light with photon energy larger than the energy band gap of Ga_2O_3, electron-hole pairs will be generated in the Ga_2O_3 nanorods.

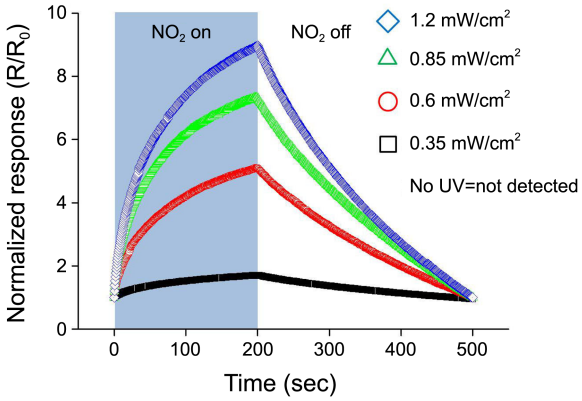

Figure 6. Dynamic responses of Pt-functionalized Ga_2O_3 nanorod gas sensors to NO_2 gas at 5 ppm for a range of UV light illumination intensities.

Table 2. Responses of the Pt-functionalized Ga_2O_3 nanorod sensor to 5 ppm NO_2 measured at room temperature for different UV illumination intensities

UV Power (mW/cm^2)	Response (%)
0.35	175.34
0.6	508.47
0.85	737.00
1.2	930.97

On their way to the surface of the Ga_2O_3 nanorods, some of the photo-generated electrons and holes will recombine each other and many remaining photo-generated holes react with negatively charged adsorbed oxygen ions on the surface as in the following reactions:[21]

$$h^+(h\nu) + O^{2-}(ads) \rightarrow O_2(g), \quad (5)$$

$$h^+(h\nu) + O^-(ads) \rightarrow 1/2O_2(h\nu), \quad (6)$$

or

$$2h^+(h\nu) + O^{2-}(ads) \rightarrow 1/2O_2(h\nu). \quad (7)$$

As a result of these reactions the surface depletion layer is reduced in the nanorods. Oxygen species are photodesorbed from the surface. On the other hand, remaining photo-generated electrons will contribute to decrease the depletion layer width and the resistance. Upon exposure to NO_2 gas, NO_2 gas adsorbs on the Ga_2O_3 nanorods and the remaining photo-generated electrons are released from the nanorods, and are attracted to the adsorbed NO_2 molecules because an oxidizing gas, such as NO_2, acts as an electron acceptor, as shown in the following reactions:[18]

$$NO_2(g) + e^-(h\nu) \rightarrow 2NO(h\nu) + O_2^-(h\nu) \quad (8)$$

This reaction widens the surface depletion region in the Ga_2O_3 nanorods, resulting in an increase in the resistance of the nanorod sensor. Therefore, the depletion layer width and the electrical resistance of the sensor increase with increasing the NO_2 concentration and UV illumination intensity because the number of electrons participating in the above reactions increases. On the other hand, after the NO_2 gas

supply is stopped, the trapped electrons are released to the Ga_2O_3 nanorod by NO_2 gas. This results in an increase in carrier concentration in the Ga_2O_3 nanorod and a decrease in the surface depletion layer width. In other words, the removed electrons are returned to the conduction band, which results in a sharp decrease in electrical resistance in the Ga_2O_3 nanorod sensors (Figure 5(b)). The significant enhancement in the response of the Ga_2O_3 nanorods to NO_2 gas by UV irradiation is attributed to the increased change in resistance due to the photo-generation of electrons and holes. In short, the significant improvement in the response of the Ga_2O_3 nanorods to NO_2 gas by UV irradiation is attributed to the increased change in resistance due to the increase in the number of electrons participating in the reactions with NO_2 molecules by photo-generation of electron-hole pairs. On the other hand, the enhancement in NO_2 gas sensing properties of Ga_2O_3 nanorods, the NO_2 gas by Pt-functionalization can be explained based on the models proposed for the metal catalyst-enhanced gas sensing of nanomaterials.[27] In the case of Pt-functionalized Ga_2O_3 nanorods, the NO_2 gas is spilt over the Ga_2O_3 nanorod surface by the Pt nanoparticles and the chemisorption and dissociation of NO_2 gas is enhanced on the Pt nanoparticle surface owing to the high catalytic or conductive nature of Pt. Consequently, the amount of electrons attracted to the gas increases. In other words, combination of the spillover effect and the enhancement of chemisorption and dissociation of gas results in the enhanced electrical response of the Pt-functionalized Ga_2O_3 nanorod sensor to NO_2 gas.

Conclusions

Pt-functionalized Ga_2O_3 nanorods were synthesized using a three-step process: the synthesis of Ga_2O_3 nanorods by the thermal evaporation of GaN powders followed by the sputter-deposition of Pt and thermal annealing. The response of the Ga_2O_3 nanorods was increased 2-3 fold at each NO_2 concentration by the functionalizing them with Pt. The response of the Pt-functionalized Ga_2O_3 nanorods increased from 189 to 619% with increasing the UV light illumination intensity from 0.35 to 1.2 mW/cm^2. The significant enhancement in the response of the Ga_2O_3 nanorods to NO_2 gas by UV irradiation is attributed to the increased change in resistance due to the photo-generation of electrons and holes. These results prove a strong influence of UV light irradiation on the response of the nanosensor to NO_2 gas. In other words, this result supports previous reports that the UV light irradiation technique can realize room temperature-gas sensors.

Acknowledgments. This study was supported by 2010 Core Research Program through the National Research Foundation of Korea (NRF) funded by the Ministry of Education, Science and Technology.

References

1. Fleischer, M.; Meixner, H. *Sens. Actuators B* **1998**, *52*, 179.
2. Frank, J.; Fleischer, M.; Meixner, H.; Feltz, A. *Sens. Actuators B* **1998**, *49*, 110.
3. Baban, C.; Toyoda, Y.; Ogita, M. *Thin Solid Films* **2005**, *484*, 369.
4. Trinchi, A.; Wlodarski, W.; Li, Y. X. *Sens. Actuators B* **2004**, *100*, 94.
5. Ohta, H.; Nomura, K.; Hiramatsu, H.; Ueda, K.; Kamiya, T.; Hirano, M.; Hosono, H. *Solid State Electron.* **2003**, *47*, 2261.
6. Xie, H.; Chen, L.; Liu, Y.; Huang, K. *Solid State Commun.* **2007**, *141*, 12.
7. Passlack, M.; Hunt, N. E. J.; Schubert, E. F.; Zydzik, G. J.; Hong, M.; Mannaerts, J. P.; Opila, R. L.; Fischer, R. J. *Appl. Phys. Lett.* **1994**, *64*, 2715.
8. Schwebel, T.; Fleischer, M.; Meixner, H. *Sens. Actuators B* **2000**, *65*, 176.
9. Ogita, M.; Higo, K.; Nakanishi, Y.; Hatanaka, Y. *Appl. Surf. Sci.* **2001**, *175*, 721.
10. Gundiah, G.; Govindarj, A.; Rao, C. N. R. *Chem. Phys. Lett.* **2002**, *351*, 189.
11. Gao, Y. H.; Bando, Y.; Sato, T. *Appl. Phys. Lett.* **2002**, *81*, 2267.
12. Kim, H.; Jin, C.; Park, S.; Kim, S.; Lee, C. *Sens. Actuators, B* **2012**, *161*, 594.
13. Arnold, S. P.; Prokes, S. M.; Perkins, K.; Zaghloul, M. E. *Appl. Phys. Lett.* **2009**, *95*, 103102.
14. Choi, Y. J.; Hwang, I. S.; Park, J. G.; Choi, K. J.; Park, J. H.; Lee, J. H. *Nanotechnol.* **2008**, *19*, 095508.
15. Zhang, Y.; Kolmakov, A.; Lilach, Y.; Moskovits, M. *J. Phys. Chem. B* **2005**, *109*, 1923.
16. Comini, E.; Cristalli, A.; Faglia, G.; Sberveglieri, G. *Sens. Actuators B: Chem* **2000**, *65*, 260.
17. Comini, E.; Faglia, G.; Sberveglieri, G. *Sens. Actuators B: Chem.* **2001**, *78*, 73-77.
18. Prades, J. D.; Diaz, R. J.; Ramirez, F. H.; Barth, S.; Cirera, A.; Rodriguez, A. R.; Mathur, S.; Morante, J. R. *Sens. Actuators B: Chem.* **2009**, *140*, 337.
19. Fan, S. W.; Srivastava, A. K.; Dravid, V. P. *Appl. Phys. Lett.* **2009**, *95*, 142106.
20. Fan, S. W.; Srivastava, A. K.; Dravid, V. P. *Sens. Actuators B: Chem.* **2010**, *144*, 159.
21. Gong, J.; Li, Y. H.; Chai, X. S.; Hu, Z. S.; Deng, Y. L. *J. Phys. Chem. C* **2010**, *114*, 1293.
22. Cao, C. L.; Hu, C. G.; Wang, X.; Wang, S. X.; Tian, Y. S.; Zhang, H. L. *Sens. Actuators B: Chem.* **2011**, *156*, 114.
23. Lupana, O.; Lee, C.; Chai, G. *Sens. Actuators B: Chem.* **2009**, *141*, 511.
24. Lu, G.; Xu, J.; Sun, J.; Yu, Y.; Zhang, Y.; Liu, F. *Sens. Actuators B: Chem.* **2012**, *162*, 82.
25. Williams, D. E. Solid State Gas Sensors, Bristol, Hilger 1987.
26. Barsan, N.; Weimar, U. *J. Electroceram.* **2001**, *7*, 143.
27. Yamazoe, N. *Catal. Surv. Asia* **2003**, *7*, 63.
28. Kolmakov, A.; Klenov, D.; Lilach, Y.; Stemmer, S.; Moskovits, M. *Nano Lett.* **2005**, *5*, 667.